Organic Electronics 14 (2013) 3297–3305

Contents lists available at ScienceDirect

Organic Electronics

journal homepage: www.elsevier.com/locate/orgel

Iridium (III) complexes with 5,5-dimethyl-3-(pyridin-2-yl) cyclohex-2-enone ligands as sensitizer for dye-sensitized solar cells

DongDong Wang [a,*], Yong Wu [a], Hua Dong [b], ZhiXiao Qin [a], Dan Zhao [c], Yue Yu [b], GuiJiang Zhou [a], Bo Jiao [b], ZhaoXin Wu [b,*], Min Gao [a], Geng Wang [a]

[a] Department of Applied Chemistry, School of Science, Xi'an Jiaotong University, Xi'an 710049, China
[b] Key Laboratory for Physical Electronics and Devices of the Ministry of Education, School of Electronic and Information Engineering, Xi'an Jiaotong University, Xi'an 710049, China
[c] Xi'an Technological University North Institute of Information Engineering, Xi'an 710025, China

ARTICLE INFO

Article history:
Received 10 August 2013
Received in revised form 5 September 2013
Accepted 30 September 2013
Available online 17 October 2013

Keywords:
Cyclohexenone
Iridium complexes
Dye-sensitized solar cell
Charge transfer

ABSTRACT

The three iridium complexes based on 5,5-dimethyl-3-(pyridine-2-yl)cyclohex-2-enone ligand and pyridine-2,4-dicarboxyl acid (**5b**) or 2,2′-bipyridine-4,4′-dicarboxyl acid (**5c**) as ancillary anchoring ligands were synthesized and characterized as potential photosensitizer for dye-sensitized solar cells (DSSC). Using of cyclohexenone derivates as ligands extended the absorption response of the iridium complex to low energy band near 550 nm and shifted the maximum emission peak to deep red (near the 680 nm). The theoretical molecular orbital calculations shows that the HOMO orbitals of all the complexes are contributed by the combination of orbitals on Ir atom (about 50%) and π orbitals located on 5,5-dimethyl-3-(pyridine-2-yl)cyclohex-2-enone. While auxiliary ligands with anchoring group exclusively contribute to electron density of the LUMO orbital, accounting for 96.33% in **5b** and 95.51% in **5c**. It is beneficial for electron injection in DSSC application. Applying them to DSSC, the IPCE response of the DSSCs covered a wide visible spectral range from 350 to 675 nm and the cells presented an open-circuit voltage of 645 mV, a power conversion efficiency of 1.03%.

1. Introduction

Dye-sensitized solar cells (DSSCs) continuously have attracted great attention because of easy fabrication and cost-effectiveness compared with silica-based photovoltaic device since pioneering research by O'Regan B. and Gratzel M. in 1991 [1]. As one of the crucial parts in DSSCs, the photosensitizers (PS) have been well developed over the past two decades and many different PS including metal complexes, porphyrins, phthalocyanines and metal-free organic dyes have been designed and applied to DSSCs. The metal complexes, in particularly ruthenium complexes [2–6], have been intensively investigated because of their broad absorption spectrum and favorable photovoltaic properties. So far, the best conversion efficiencies have been achieved with ruthenium-based sensitizers except for recently reported the best efficiency of 12.7% with donor-π-bridge-acceptor zinc porphyrin dye [7]. The light absorption of this type of complexes in visible part of solar spectrum is mainly due to MLCT (metal-to-ligand charge transfer) process, which is very sensitive to the spatial separation (r) with electrode surface. Upon optical excitation, the electrons in TiO_2 film injected from dyes are inclined to recombination with a redox couple presented in electrolyte. Also, isothiocyanate ligand (−NCS) usually includes the most of Ru-based complexes using for raise the HOMO energy of the complex, and the monodentate ligand

* Corresponding authors. Tel./fax: +86 202982663914 (D. Wang), tel.: +86202982664867.
E-mail addresses: ddwang@mail.xjtu.edu.cn (D. Wang), zhaoxinwu@mail.xjtu.edu.cn (Z. Wu).

1566-1199/$ - see front matter © 2013 Elsevier B.V. All rights reserved.
http://dx.doi.org/10.1016/j.orgel.2013.09.040

appears to be unfavorable to the stability of the materials [8,9]. Thus, the dilemma for Ru-based cells is that their conversion efficiency fluctuated at a range of 11–12% in recent years [4,10].

Iridium complexes have been widely investigated in the past two decades for their practical applications in organic light-emitting devices because of high photoluminescence quantum yields and excellent color tunability [11–14]. In 2006, it has been first demonstrated as sensitizer in DSSC to produce current by LLCT (ligand to ligand charge transfer) process [15], which is favorable to the suppress of charge recombination. Up to now, there are only few published papers on iridium complexes as sensitizer in DSSC [16,17] and cell parameters reported in these papers are not very good. However, despite poor characteristics of these cells compared with the usually used Ru-based cells, iridium complexes have been suggested to have great promising application in DSSC due to several advantages such as having the possibility for dual sensitization through LLCT and MLCT process, less accessible MC (metal-centered) state and thus higher stability [18]. Unfortunately, the development of iridium complex for this purpose is in their infancy for a main barrier that their absorption response is exclusively located at a UV or blue region, little overlapping with the radiant energy of sun light. So, improving their absorption responses in visible light range is a top concern for iridium complex to be applied to DSSC fields.

Recently, several strategies performed intended to improve the absorption response of iridium complexes, such as modifying phenylpyridine ligand with oligothiophene pendants [19], oligofluorene segment [20] or using 7-diethyaminocoumarine auxiliary ligand [21]. These endeavors only induced significantly enhanced absorption response in wavelength range from 400 to 500 nm. Just recently, we demonstrated that introducing of dicyanovinyl unit into phenyl *meta*-position of ppy (phenylpyridine) in iridium (III) bis(phenylpyridinato)picolinate can induced a significantly enhanced absorption capacity in the visible light range from 400 to 500 nm and used them as co-sensitizer with N719, notably improved cell parameters have been observed. In addition, we noticed that alkenylpyridines-based iridium complexes showed a more wide absorption response than 2-arylpyridine or 2-arylquinolines and -isoquinolines did in visible light range [22–24].

In this paper, we report three new iridium complexes using 5,5-dimethyl-3-(pyridin-2-yl)cyclohex-2-enone as cyclometalation ligands for DSSC (Fig. 1). The newly designed iridium complexes are expected to have a wide absorption response in visible light range and suppressed triplet–triplet (T–T) annihilation when anchored on TiO_2 film because of using rigid and bulky cyclohexenone ligands.

2. Results and discussion

2.1. Synthesis, UV and emission spectra

The synthesis route of the three complexes is shown in Scheme 1. The ligand (3) was prepared by treating 2-bromopyridine with n-butyllithium at −78 °C, and then by 5,5-dimethyl-3-Ethoxy-cyclohex-2-enone (2) in 28% yields. Here, the intermediate (2) was prepared by etherifying enol of 5,5-dimethyl-1,3-cyclohexanedione with ethanol in the presence of p-toluenesulfonic acid. The desired complex **5a**, **5b** and **5c** were prepared according to our previously published procedure [25]. Typically, the chloro-bridged iridium(III) dimmer directly reacted with sorts of auxiliary ligands 2,2′-bipyridine-4,4′-dicarboxylic acid or picolinic acid/pyridine-2,4-dicarboxylic acid in proper solvent to provide the desired final product.

The UV-vis absorption and photoluminescence spectra of **5a**–**5c** measured in CH_3CN solution are presented in Fig. 2, as well as absorption spectra of **5b** and **5c** on TiO_2 film, and corresponding spectra data are summarized in Table 1. Fig. 2(a) indicates that the three iridium complexes own wide absorption response in visible light range and absorption bands with significant intensity extend to about 550 nm, which is very interesting for DSSC application. A slight blue-shifted absorption response was observed in the spectra of complex **5c** compared with that of the complex **5a** and **5b**. These phenomenons have been ever observed in several iridium complexes when auxiliary ligands picolinic acid/pyridine-2,4-dicarboxylic acid was replaced by 2,2′-bipyridine-4,4′-dicarboxylic acid in our research. The UV-region, 250–350 nm, shows a strong absorption band, that can be assigned to π–π^* intra ligand absorption for 5,5-dimethyl-3-(pyridin-2-yl)cyclohex-2-enone and sorts of auxiliary ligands. The near-visible and visible region between 350 and 550 nm was occuppied by a flat absorption band with considerably intensive extinction coefficient. This could be attributed to MLCT transition (metal-to-ligand charge transfer) or LLCT transition. The absorption spectra of **5b** and **5c** on TiO_2 film are similar with that in CH_3CN.

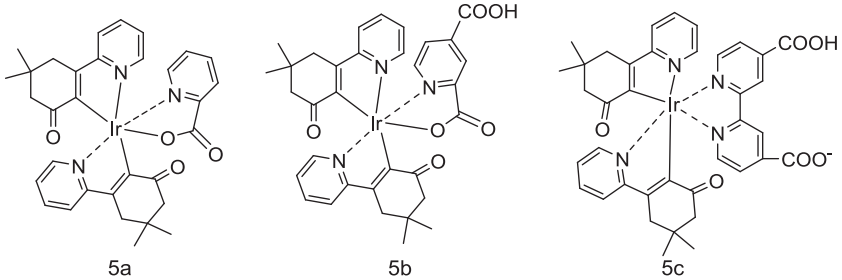

Fig. 1. Schematic structure of the synthesized iridium complexes.

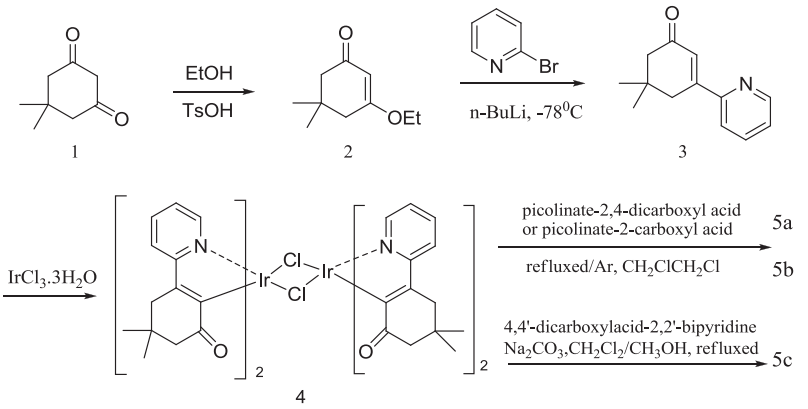

Scheme 1. The synthesis route of iridium complexes **5a**–**5c**.

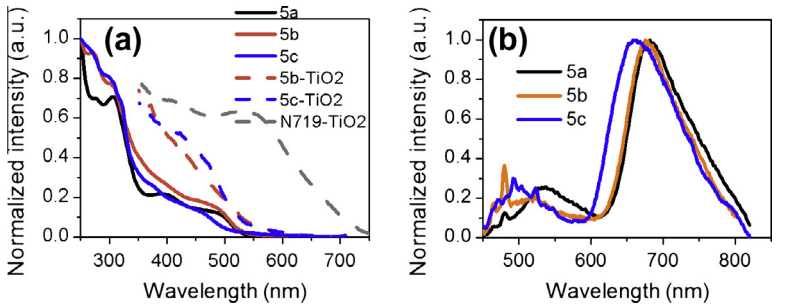

Fig. 2. (a) The absorption and (b) photoluminescence spectra of the iridium complexes **5a**–**5c** in CH_3CN solution, as well as absorption spectra of **5b** and **5c** bounded to TiO_2 film in figure (a).

Table 1
The photophysical properties of the iridium complexes.

	$\lambda_{max,abs}$ (nm)[a]	$\lambda_{max,PL}$ (nm)[a]	$E_{1/2(ox)}$, (V)[b]	HOMO[c]/LUMO[d]
5a	306, 393, 493	682	0.58	5.38/3.33
5b	273, 300, 491	675	0.54/1.04[e]	5.34/3.30
5c	290, 465	658	0.65/0.83[e]	5.45/3.42

[a] Measured in CH_3CN at 1×10^{-6} M.
[b] For complexes **5a** and **5b**, measured in CH_2Cl_2 solution of 1×10^{-6} M and for complex **5c** measured in DMSO solution, the potentials were corrected according to the potential of Fc^+/Fc and the potential value is relative to Fc^+/Fc.
[c] The HOMO energy level was estimated with the following formula: $HOMO(eV) = E_{1/2(OX)} + 4.80$.
[d] LUMO = HOMO – Δ_G (the absorption onset estimated from absorption spectrum in CH_3CN solution.
[e] The oxidation potential of the complexes **5b** and **5c** loaded on TiO_2 film relative to Fc^+/Fc.

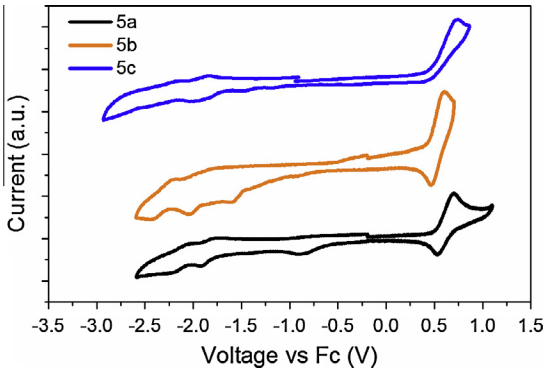

Fig. 3. The cyclic voltammograms of the iridium complexes **5a**–**5c** (the positive scan for complex **5a** and **5b** were performed in CH_2Cl_2 solution and the negative scan for all the complexes were carried out in DMSO, as well as positive scan of the complex **5c**).

Upon optical excitation, the three complexes **5a**, **5b** and **5c** show deeply red emission with a peak value of 682, 675 and 658 nm, respectively. These emission energy are significantly lower than that of ever reported iridium complex with 2-cycloalkenyl pyridine ligands (about 535 nm), [24] indicating introducing of carbonyl group into 2-cycloalkenyl pyridine extended π conjugated system and shifted their emission to lower energy side. Being similar to their absorption profiles, a slightly blue-shifted emission was observed in complex **5c** comparing with that in complex **5a** and **5b**. In addition, a weak emission near 500 nm was observed for three complexes and the reasonable cause for this cannot be provided at the moments.

2.2. Electrochemistry

Cyclic voltammogram (CV) of three complexes were examined in DMSO for negative scan and in CH_2Cl_2 for positive scan with Fc^+/Fc as internal standard, as well as

dye-loaded TiO_2 film. The CV curves were corrected according to the potentials of the Fc^+/Fc and are shown in Fig. 3 and the curves of the dye-loaded TiO_2 film are presented in Fig. S5 (see Supporting information). The voltammograms show Ir(IV)/Ir(III) oxidated couple at positive potentials and ligand-based reduction couple at negative potentials. Some of the electrochemical data are presented in Table 1. For the complexes **5a** and **5b**, the well reversible redox peaks in solution were observed at about 0.58 and 0.54 V vs Fc^+/Fc, respectively, assigned to the Ir(IV)/Ir(III) couple. But, the oxidation peak of the complex **5c** in CH_2Cl_2 or CH_3CN solution failed to be observed at positive scan, and alternatively, an irreversible oxidation peak at 0.65 V vs Fc^+/Fc was observed in DMSO solution. The higher oxidation potential of the complex **5c** is due to the lower electron densities on the metal central, mainly caused by the ligand field effect of 2,2′-bipyridine-4,4′-dicarboxylic acid. In addition, we noticed that the oxidation potentials of the **5b** and **5c** sensitizer absorbed on TiO_2 films are 1.04 and 0.83 V vs Fc^+/Fc, slightly higher than that in solution. The oxidation potentials of all the complexes are more positive than that of I^-/I_3^- redox couple (0.4 V vs NHE), benefitting to regenerate iridium complexes in I^-/I_3^- electrolyte [26]. Based on the measured oxidation potentials in solution, the HOMO energy levels were determined and shown in Table 1. On the other hand, the three complexes exhibit several irreversible reduction processes whether in solution or dye-loaded TiO_2 films. Their first reduction peak occurred at −1.90, −1.59 and −1.96 V vs Fc^+/Fc for complexes **5a**, **5b** and **5c** in solution, respectively, while −1.81 and −2.45 V vs Fc^+/Fc in dye-loaded TiO_2 film. These values are more negative than that of the conduction-band edge of TiO_2 (−0.5 V vs NHE at PH = 7), benefiting electron injection from these excited states to TiO_2. The irreversible reduction process is poorly reliable for the direct determination of the LUMOs energy levels from CV measurements. So, the optical LUMOs energy was calculated as shown in Table 1.

2.3. DFT calculations

To gain more insight into the electrochemical and photophysical behaviors of all these cyclohexenone-based iridium complexes, we performed molecule orbital (MO) calculations. The HOMOs and LUMOs orbitals of electronic ground states for the iridium complexes are shown in Fig. 4 and other orbitals are presented in Fig. S2-4 (see Supplementary Information). For all three complexes, HOMO molecular orbitals has an important Ir(**5d**) contribution of 44.73% in **5a**, 44.47% in **5b** and 41.27% in **5c**. The remain contributions mainly come from orbitals located on both 5,5-dimethyl-3-Ethoxy-cyclohex-2-enone ligands (52.06% in **5a**, 52.08% in **5b** and 56.92% in **5c**). Be similar to the HOMO, the HOMO-1, HOMO-2 orbitals of all the complexes are contributed by the combination of orbitals on Ir atom and π orbitals located on cyclohexenone. But, the proportion of Ir(**5d**) orbital in **5a** (>51%) and **5b** (>48%) slightly increased while that in **5c** decreased slightly (<42%). For the LUMO orbitals, it is interesting to find that cyclohexenone ligand presents a main contribution in **5a**, 73.89% in LUMO and 72.36% in LUMO+1 orbital while auxiliary ligands 2,2′-bipyridine-4,4′-dicarboxylic acid in **5c** present a dominant contribution, accounting for 95.51% in LUMO and 98.37% in LUMO+1 orbital, respectively. In addition, pyridine-2,4-dicarboxylic acid contributed 96.33% to the LUMO orbital of **5b**. This means that introducing of anchoring unit carboxyl group into picolinic acid or replacing it with 2,2′-bipyridine-4,4′-dicarboxylic acid induce a distinct redistribution of electron density among ligands and as a result, it is benefiting for electron injection in DSSC application.

The Fig. 5 shows predicted UV-vis absorption spectra calculated by time-dependent density functional theory (TD-DFT) only considering the vertical singlet state transition in CH_2Cl_2. The transitions with significant oscillator strength are summarized in Table S1 (see Supporting Information). It can be seen that the calculated absorption spectra generally coincides to the experimental absorption. The three complexes all present a common first transition of HOMO→LUMO type (**5a**: 477.6 nm, **5b**: 512.6 nm, **5c**: 568.1 nm). On the basis of the DFT/TDDFT calculations, the electron transition in the spectra range from 350 to 600 nm, which primarily involved molecular orbitals HOMO-0/1/2 and LUMO+0/1/2, are attributed to MLCT and/or LLCT transition for the complexes **5a**–**5c**. As for strong absorption bands observed in the UV region (below 350 nm), the orbitals HOMO-4 or 5 (where electron density are mainly located on cyclohexenone unit) and LUMO+4 or 5 (where electron density are primarily located on pyridine ring), are generally involved in the transition processes, and therefore $\pi \rightarrow \pi^*$ transitions from intra-ligands are mainly contributed to the absorption response in this region.

2.4. DSSCs performance

To evaluate the application potentiality of these iridium complexes in DSSCs, the DSSCs with usual configuration were fabricated and donated as device **5b** and **5c**. The N719-sensitized DSSC was also fabricated for a fair comparison. In these DSSCs, a mixture of acetonitrile and valeronitrile (volume ratio, 85:15) including 0.6 M 1-butyl-3-methyl imidazolium iodide (BMII), 0.03 M I_2, 0.02 M LiI, 0.10 M guanidinium thiocyanate and 0.5 M 4-tert-butylpyridine were used as the redox electrolyte. The photovoltaic performances of these solar cells were measured under AM 1.5G conditions (100 mW/cm^2). Their photocurrent-voltage and IPCE (the incident monochromatic photo-to-current conversion efficiency) curves are shown in Fig. 6. It can be seen that the IPCE curves for the **5b** and **5c**-based DSSCs exhibited common broadening characteristics that covered spectral range from 350 to 675 nm, with notable peaks at 530 nm for **5b** and 550 nm for **5c**. This result indicates that it is possible for iridium complex to achieve entire visible light-harvesting response (from 350 to 800 nm) as that usually used Ru-dyes in DSSC. Notably, both solar cells based on iridium dyes **5b** and **5c** give similar open-circuiting voltage (Voc), 645 and 626 mV, respectively, about 100 mV higher than that of the early reported results that used iridium complexes as photosensitizer [15–17]. However, these DSSCs produced low photocurrent density, such as 2.1 mA cm^{-2} for **5b**, and 1.8 mA cm^{-2} for **5c**, respectively, corresponding to overall conversion

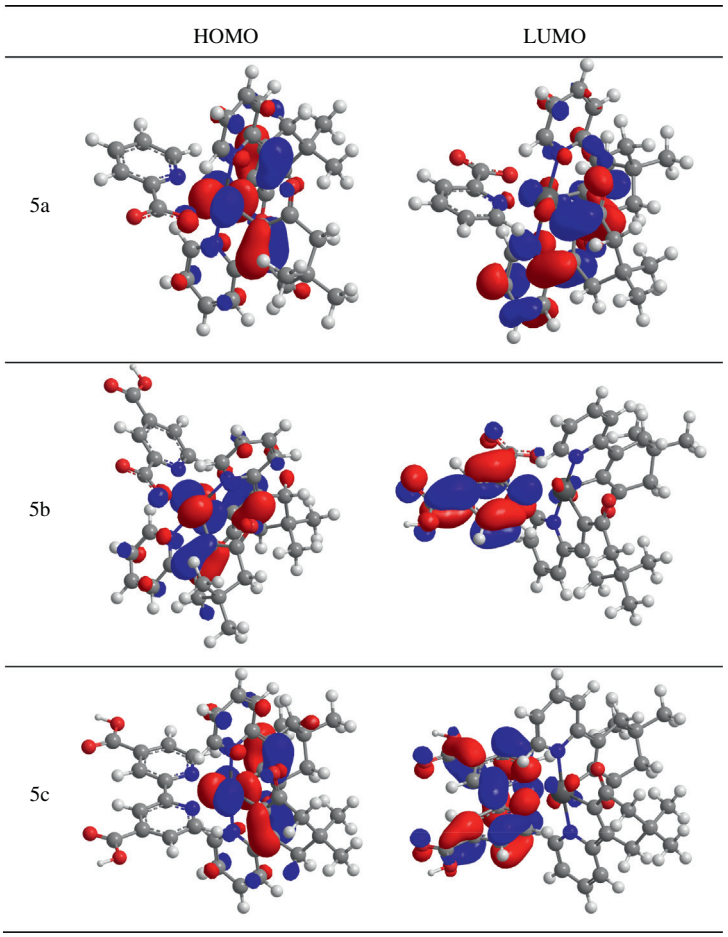

Fig. 4. The calculated contours of the HOMOs and LUMOs orbitals of the iridium complexes **5a**–**5c**.

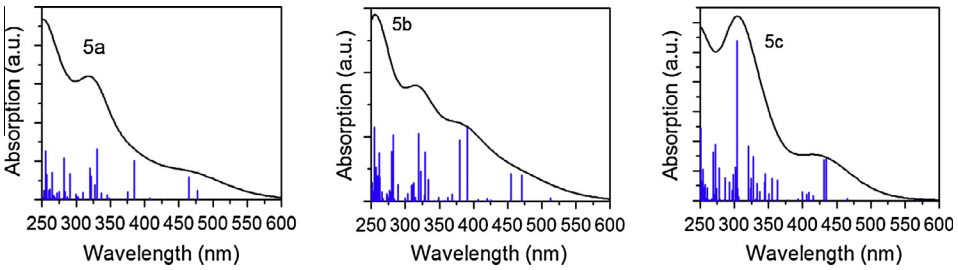

Fig. 5. Absorption spectra of iridium complexes **5a**–**5c** are predicted by TDDFT/M06. (Simulated absorption spectra donated by black lines and singlet vertical excitation energies represented by blue bars.) (For interpretation of the references to colour in this figure legend, the reader is referred to the web version of this article.)

efficiencies of 1.03% and 0.83%, respectively. These values are significantly lower than that of N719-based DSSC (6.08%).

To get insight into the charge transfer processes in DSSCs based on different dyes, the electrochemical impedance spectroscopy (EIS) of DSSCs were investigated. In this work, the EIS spectrum of the devices **5b** and **5c** were measured at V_{oc} of the DSSCs under 1.5 AM full light, and the Nyquist and Bode phase plots are shown in Fig. 7a and b, respectively. In our EIS spectrum, the second response peaks for **5b** and **5c**-based DSSCs, corresponding to electron transport and recombination in the TiO_2, [27] are significantly different. As shown in Fig. 7a, the radius of the second semicircle are in the order, **5c** > **5b**, indicating that the charge recombination rate increased in the order **5c** < **5b**. In Fig. 7b, the frequency peak for the second semicircle is indicative of charge-transfer process of injected electron in TiO_2, which increased along **5b** (3.15 Hz) to **5c** (5.01 Hz), corresponding to a decrease of electron lifetime along the order. This is because the

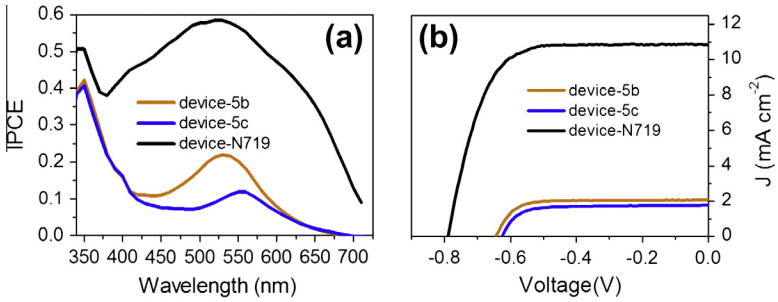

Fig. 6. (a) IPCE spectra and (b) photocurrent density–voltage characteristics curves for DSSC devices recorded under illumination of simulated solar light (AG 1.5G, 100 mW/cm^2).

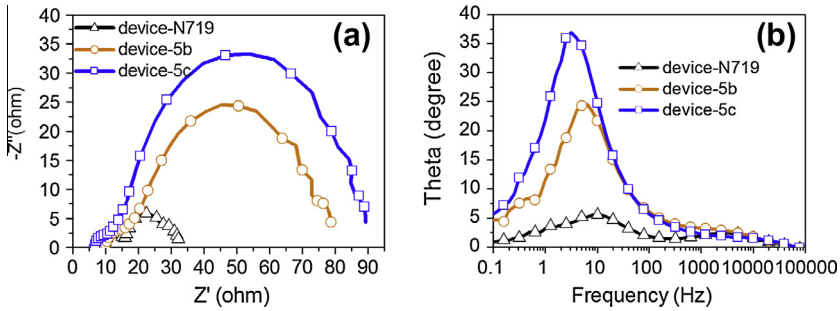

Fig. 7. EIS spectra of DSSCs based on different iridium complexes measured under AM 1.5G conditions (100 mW cm^{-2}) at a bias of −0.62 V, (a) Nyquist and (b) bode phase plots.

electron lifetime can be obtained from meddle frequency peak using the equation $\tau_e = 1/2\pi f$, in which f is frequency peak. It is usually acceptable that an increase in electron lifetime at the second semicircle is correlated with an increase in V_{oc} of EIS [28]. So, the longer electron lifetime of **5b**-based cell explained its relatively higher V_{oc} in comparison with **5c**-based cell.

In our opinion, although the photovoltaic performances of DSSCs with these iridium complexes was lower than that of the DSSC with ruthenium complex dye, the potential of iridium complexes as a sensitizer for DSSCs have been well indicated. The inferior cell parameters may be mainly related with poor absorption response of these iridium complexes in visible region, and improving their absorption properties are expected to improve the short-circuit current of the cells, resulting in useful power conversion efficiencies. For this purpose, using ligands with extended π – conjugation length would be warrant to achieve better light-harvesting performances, such as replacing pyridine unit of the present iridium complexes with benzothiazole or quinoline derivates. Moreover, changing electron density of the ligands by employing attached substitutes can also produce iridium complexes that feature intense absorption and broader spectral response in the visible region. For example, we recently found that introducing of dicyanovinyl substituent into phenyl *meta*-position of ppy (phenylpyridine) in iridium (III) bis(phenylpyridinato)picolinate induced a significant enhancement of absorption response ranged from 400 to 500 nm [25]. Furthermore, replacing dicyanovinyl with 2-(2-methyl-6-vinyl-4H-pyran-4-ylidene)malononitrile unit can extend absorption capacity of the resulting iridium complexes to 650 nm (unpublished data). In addition, introducing strong absorbing chromophores such as oligothiophene [19] or oligofluorene [20] as substitutes to ppy in iridium complexes can also induce an enhanced absorption response in visible light region. On the other hand, those iridium complexes in present study or others are expected to have a LUMO localized on the bipyridine or pyridine-2,4-dicarboxyl acid ligands. However, when the anchoring carboxyl group is directly attached to the main ligands, the cell characteristics have been dramatically improved [18]. Maybe, this concept is very helpful for rational structural modification or molecular design of the iridium complexes for DSSCs. Above all, the basic principles and common characteristics of triplet emission in iridium complexes have been well established. However, the structure–photovoltaic property relationship of the iridium complexes is obscure and less understood. This needs to be intensively investigated in the future and thus the unique features of the iridium complexes would actually promote development of DSSCs application.

3. Conclusion

In summary, we have synthesized and characterized a new series of iridium complexes with 5,5-dimethyl-3-(pyridin-2-yl)cyclohex-2-enone as cyclometalation ligands and pyridine-2,4-dicarboxyl acid or 2,2′-bipyridine-4,4′-dicarboxyl acid as ancillary ligands. These iridium complexes based on cyclohexenone derivates as main ligand

show wide absorption response in visible light range and deeply red emission while aryl-pyridine-based iridium complexes usually present a UV or blue absorption response and green/yellow emission. The theory calculation suggest that the electron density of LUMO orbitals of the complexes with carboxylic acid are exclusively located on auxiliary ligands pyridine-2,4-dicarboxylic acid or 2,2′-bipyridine-4,4′-dicarboxylic acid. This property would be greatly beneficial to the electron injection from excited states of the dye molecules to TiO_2. Using these iridium complexes as photosensitizer, the fabricated DSSCs exhibit a widely responding IPCE characteristic and a V_{oc} of 645 mV, but only 1.08% conversion efficiency. The inferior cell parameters may be related with poor absorption response of these iridium complexes in visible region. Although the cell parameters could not compete with Ru-based DSSCs presently, the IPCE response of the iridium complexes-based DSSCs covered wide spectral range from 350 to 675 nm, which is ever considered as difficult to achieve. This result indicates that it is possible for iridium complexes to be widely used as photosensitizer in DSSCs fields as that in OLED fields to achieve full visible spectra response cells with significantly high energy conversion efficiency if more attentions are put on the subject. Thus, the dual sensitization property and the well electrochemical stability of the iridium complexes would be greatly beneficial to the improvement of the cell parameters in comparison with Ru complexes.

4. Experimental section

4.1. Spectroscopy and CV

The steady-state absorption and emission spectra were recorded with Hitachi (U-3310) spectrophotometers and Edinburgh (FS920) fluorometers, respectively. The absorption spectra of the dyes adsorbed on TiO_2 films were measured with a Varian Cary 500 spectrophotometer.

Cyclic voltammetry (CV) measurements were performed on a Princeton applied research model 273 A electrochemical workstation. The oxidation and reduction measurements were recorded using a glassy carbon as working electrode, Pt-sheet and Pt-wire as counter electrode and reference electrode, respectively. As for measurements of dye-loaded on TiO_2 film, the dye-sensitized TiO_2 film on conducting glass as the working electrode, CH_3CN as solvent, and the scan rate is 50 mV s^{-1}. For the positive scan, the experiments were performed in anhydrous CH_2Cl_2 solution containing 0.1 M TBAPF6 and for negative scan, DMSO solution was used. The potential were measured against Pt-wire reference electrode with ferrocenium/ferrocence (Fc/Fc^+) as internal standard and the scan rate is 100 mV s^{-1}.

4.2. The preparation and measurement of DSSCs

The glass substrates coated FTO (Nippon Sheet Glass, Japan, 2.2 mm thickness,14 Ω/□) were cleaned in a detergent solution for 30 min with an ultrasonic bath, rinsed with deionized water for 30 min, isopropanol and EtOH for 30 min, respectively. A first transparent layer was screen-printed with a transparent TiO_2 paste (P90 Degussa..15-nm), then the coated films were dried at temperature of 125 °C for 6 min. This screen-printing procedure with the paste was repeated to obtain an appropriate thickness of 12 μm of TiO_2 for the working electrode. On the electrode of TiO_2, a 5 μm thickness light-scattering layer containing 200 nm sized anatase of TiO_2 was also deposited by screen-printing. The coated substrates were thermally treated under an air flow at 325 °C for 5 min, 375 °C for 10 min, 450 °C for 15 min and 500 °C for 15 min in sequence, and the heating ramp rate was 5–10/min. The sintered layer was treated again with 40 mM/L titanium tetrachloride-aqueous solution (70 °C for 30 min), rinsed with water and EtOH and heated at 450 °C for 30 min. After cooling down to 80 °C the TiO_2 electrode was stained by immersing it into a dye solution containing iridium complex or N719 sensitizer (300 μM) and cheno (2 mM) in a mixture of CH_2Cl_2:CH_3OH (volume ratio: 4/1) for 20 h. The dye absorbed TiO_2 electrode and Pt nanoparticle-structured counter electrode were assembled into a sealed sandwich-type cell by a 60 μm hot-melt ionomer film Bynel (Dupont) as a spacer between the electrodes. Then, the electrolyte solution was added to the hole and introduced inside the cell. Finally, the hole was sealed with a hot-melt ionomer film Bynel and a cover glass, the active area of the cell was typically 0.25 cm^2. The electrolyte used for device **5b**–**5c** and N719 contains 0.6 M 1-butyl-3-methyl imidazolium iodide (BMII), 0.03 M I_2, 0.02 M LiI, 0.10 M guanidinium thiocyanate and 0.5 M 4-tert-butylpyridine in a mixture of acetonitrile and valeronitrile (volume ratio, 85:15).

The current–density voltage (*J*–*V*) characteristics of the DSSCs were measured by recording *J*–*V* curves using a Keithley 2400 source meter under the illumination of AM 1.5 G simulated solar light (Newport-91160 equipped with a 300 W Xe lamp and an AM 1.5 G filter). The incident light intensity was calibrated to 100 mW cm^{-2} with a standard silicon solar cell (Newport 91150V). Action spectra of the incident monochromatic photonto-electron conversion efficiency (IPCE) for the solar cells were obtained with a Newport-74125 system (Newport Instruments). The intensity of monochromatic light was measured with a Si detector (Newport-71640).The electrochemical impedance spectroscopy (EIS) measurements of all the DSSCs were performed using a CHI-660D at V_{oc}. The frequency range is 0.1 Hz–100 kHz and the applied voltage bias is −0.62 V. The magnitude of the alternative signal is 10 mV.

4.3. The synthesis of the iridium complexes

All the reactions were carried under an argon atmosphere and reagents were used without further purification. The ^1H NMR and ^{13}C spectra were recorded on Bruker Advance 400 MHz spectrometers and HRMS experiments were carried out on a Thermo Scientific LTQ Orbitrap Discovery (Bremen, Germany).

4.3.1. 5,5-Dimethyl-3-Ethoxy-cyclohex-2-enone (2) [29]

P-toluenesulfonic acid (0.200 g, 1.05 mmol) was added to a stirred solution of 5,5-dimethyl-1,3-cyclohexanedione

(7.8 g, 56 mmol) in EtOH (25 mL) and PhMe (90 mL) at room temperature. Subsequently, the reaction mixture was heated at reflux and traced with TLC until it was completed about 12 h. The reaction mixture, then, was cooled to room temperature and concentrated in vacuo to give an orange oil. The crude material was dissolved in EtOAc (100 mL) and neutralized with 1 M NaOH (25 mL). The resulting solution was partitioned with H_2O (100 mL) and extracted with EtOAc (3 × 100 mL). The combined organic layers were dried over $MgSO_4$ and concentrated in vacuo to afford intermediate 2 as an orange oil that was used without further purification. (2.93 g, Yield 31.2%) ^{1}H NMR (400 MHz, CD_3Cl-d_3, δ): 5.346 (s, 1H), 3.905–3.923 (t, 2H, $-CH_2-O$), 2.285 (s, 2H, $-CH_2-$), 2.212 (s, 2H, $-CH_2-$), 1.375 (tri, 3H, $-CH_3$), 1.082 (s, 6H, 2-CH_3); ^{13}CNMR (400 MHz, CD_3Cl-d_3, δ): 199.15, 175.92, 101.26, 64.03, 50.58, 42.73, 32.27, 28.12, 13.99; MS: m/z 170 [M^+].

4.3.2. 5,5-dimethyl-3-(pyridin-2-yl)cyclohex-2-enone (3)

To a THF solution (40 mL) of 2-bromopyridine (5.5 g, 34.7 mmol) was added dropwise a solution of n-BuLi (2.5 M, 13.7 mL, 34.9 mmol) in hexane at −78 °C. After stirring for 2 h at 0 °C, the mixture was cooled to −78 °C, followed by addition of 5,5-dimethyl-3-Ethoxy-cyclohex-2-enone 2 (2.93 g, 17.2 mmol) and the mixture was stirred at room temperature overnight, then treated with 2 M HCl solution. The diethyl ether layer was concentrated and eluted through a silica column to afford 5,5-dimethyl-3-(pyridin-2-yl)cyclohex-2-enone (3): (0.98 g, Yield 28.0%) ^{1}H NMR (400 MHz, CD_3Cl-d_3, δ): 8.702–8.713 (m, 1H), 7.756–7.775 (d, J = 7.6 Hz, 1H), 7.666–7.685 (d, J = 7.6 Hz, 1H), 7.314–7.344 (m, 1H), 6.782 (s, 1H), 2.857 (s, 2H), 2.391 (s, 2H), 1.160 (s, 6H); ^{13}C NMR (400 MHz, CD_3Cl-d_3, δ): 200.77, 156.54, 156.12, 149.52, 136.77, 125.80, 124.16, 121.27, 51.29, 40.38, 33.56, 28.41; MS: m/z 201[M^+].

*4.3.3. Synthesis of the complexes **5a** and **5b***

A mixture of the ligand 3 (0.98 g, 7.5 mmol), $IrCl_3 \cdot 3H_2O$ (0.6 g, 2.0 mmol), 2-ethoxyethanol (24 mL)/distilled H_2O (8 mL) was refluxed under argon for 24 h. After cooling to room temperature, distilled H_2O (150 mL) was added and the resulting precipitate was collected by filtration and washed with water and hexane successively. After drying, the 0.65 g crude product was obtained, which was directly used for next step without further purifying.

A solution of the dimer (0.5 g, 0.398 mmol) and pyridine-2-carboxyl acid (0.12 g, 0.996 mmol) in 1,2-dichloroethane (60 mL) was refluxed under argon for 28 h, then 1,2-dichloroethane was evaporated and the resulting precipitate was directly dissolved in mixed solvent of CH_3OH/CH_2Cl_2 (1:3) and recrystalled to afford the desired iridium complexes. Finally, the product was subjected to flash column chromatography to afford pure product **5a**: (0.25 g, Yield 35%) ^{1}H NMR (400 MHz, $CDCl_3$-d, δ): 8.628–8.612 (d, J = 6.4, 1H), 8.306–8.324 (d, J = 7.2, 1H), 8.085–8.097 (d, J = 4.8, 1H), 7.909–7.951 (t, 1H), 7.632–7.674 (t, 2H), 7.374–7.442 (m, 4H), 7.034–7.070 (t, 1H), 6.860–6.897 (t,1H), 2.625–2.671 (d, 3H), 2.460–2.501 (d, 1H), 2.235–2.320 (m, 3H), 1.993–2.030 (d, 1H), 1.144 (s, 3H), 1.077 (s, 3H), 1.017 (s, 3H), 0.874 (s, 3H); ^{13}CNMR (400 MHz, $CDCl_3$-d, δ):204.94, 204.70, 173.01, 170.13, 169.49, 153.88, 153.60, 151.73, 148.88, 148.81, 148.76, 146.75, 145.65, 137.84, 136.62, 136.43, 128.39, 128.14, 121.85, 121.62, 120.80, 120.28, 52.96, 52.74, 40.44, 40.38, 34.03, 33.79, 29.91, 28.79, 28.72, 27.36; HRMS (ESI): calc. for $C_{32}H_{32}IrN_3O_4$, 715.2022; found: 716.2081 ([M + H]$^+$).

The dimer and pyridine-2,4-dicarboxylacid are 0.4 g (0.32 mmol) and 0.13 g (0.80 mmol), respectively. The pure product was obtained by flash column chromatography. **5b** (0.20 g, Yield 53%): ^{1}H NMR (400 MHz, DMSO-d_6, δ): 8.928 (s, 1H), 8.563–8.577 (d, J = 5.6, 1H), 8.240–8.253 (d, J = 5.2, 3H,), 8.012–8.030 (d, J = 5.6, 2H), 7.661–7.700 t, 2H), 7.410–7.444 (t, 2H), 7.360–7.372 (d, J = 4.8, 1H), 7.065–7.100 (t, 1H), 6.895–6.931 (t, 1H), 2.736 (s, 4H), 2.694 (s, 2H), 2.260 (s, 2H), 1.154 (s,3H), 1.074 (s, 3H), 1.015 (s, 3H), 0.888 (s, 3H); ^{13}CNMR (400 MHz, DMSO-d_6, δ):204.90, 204.86, 173.15, 169.86, 169.17, 164.50, 154.36, 154.18, 152.30, 149.80, 148.82, 145.90, 139.80, 136.97, 136.82, 128.44, 122.25, 122.00, 121.01, 120.61, 52.89, 52.68, 40.40, 34.05, 33.80, 29.69, 28.84, 28.58, 27.48; HRMS (ESI): calc. for $C_{33}H_{32}IrN_3O_6$, 759.1920; found: 760.1980 ([M + H]$^+$).

*4.3.4. Synthesis of the complex **5c***

The dimer of $Ir_2(C^\wedge N)_4Cl_2$ (0.25 g, 0.2 mmol) and 4,4′-dicarboxylacid-2,2′-bipyridine (0.122 g, 0.50 mmol) were dissolved in CH_3OH/CH_2Cl_2 (60 mL, 1:3,v/v), and then excessive Na_2CO_3 (0.7 g, 6.63 mmol) was added. The reaction mixture was heated at reflux under argon for 24 h and the solvent was removed on a rotary evaporator under vacuum. The resulting suspended solution was poured into water and acidified to a PH of approximately 5.0 with 0.5 M HCl solution. The crude product was obtained in a precipitate form and purified by recrystallization using CH_3OH/CH_2Cl_2 (1:3) as mixed solvent to afford the desirable complex **5c**. Finally, the product was subjected to flash column chromatography to afford pure product **5c**. (0.16 g, Yield 61.5%) ^{1}H NMR (400 MHz, DMSO-d_6, δ): 8.734 (s, 2H), 8.174–8.188 (d, J = 5.6 Hz, 2H), 8.515–8.480 (m, 4H), 7.854–7.868 (J = 5.6 Hz, 2H), 7.718–7.756 (t, 2H), 7.566–7.586 (d, J = 8.0 Hz, 2H), 7.358–7.372 (d, J = 5.6 Hz, 2H), 6.932–6.965 (t, 2H), 2.760–2.802 (d, 2H), 2.564 (s, 2H), 2.376−2.413 (d, 2H), 1.978–2.015 (d, 2H), 1.116 (s, 6H), 0.890 (s, 6H); ^{13}CNMR (400 MHz, DMSO-d_6, δ):203.24, 169.04, 164.59, 155.43, 154.01, 152.42, 150.70, 149.40, 149.22, 137.74, 127.97, 123.77, 123.38, 121.81, 53.12, 33.95, 29.84, 27.63; HRMS (ESI): calc. for $C_{38}H_{36}IrN_4O_6$, 837.2264; found: 837.2242 ([M$^+$]).

4.4. Computational details of theoretical calculations

Singlet ground state (S_0) geometries of all relevant iridium compounds were fully optimized by using M06 method of density functional theory (DFT). The standard 6-311G(d,p) basis set on non-metal atoms and the relativistic effective core potential (ECP) LANL2DZ on Ir atom were taken in our calculations. The solvent effects were evaluated with the self-consistent reaction field (SCRF) based on the integral equation formalism of the polarizable continuum model (IEFPCM) in CH_2Cl_2 solvent (ε = 8.93). The vertical excitation calculations in CH_2Cl_2

for the simulation of absorption spectra were used by the time-dependent (TD) DFT method. All calculations were carried out with the Gaussian 09 program package.

Acknowledgements

This work has been supported by the Fundamental Research Funds for the Central Universities (Grant. No. 08143034), the Basic Research Program of China (2013CB328705), National Natural Science Foundation of China (Grant Nos. 61275034 and 61106123).

Appendix A. Supplementary material

Supplementary data associated with this article can be found, in the online version, at http://dx.doi.org/10.1016/j.orgel.2013.09.040.

References

[1] B. Oregan, M. Gratzel, Nature 353 (1991) 737.
[2] P. Wang, S.M. Zakeeruddin, J.E. Moser, M.K. Nazeeruddin, T. Sekiguchi, M. Gratzel, Nature Materials 2 (2003) 402.
[3] M.K. Nazeeruddin, F. De Angelis, S. Fantacci, A. Selloni, G. Viscardi, P. Liska, S. Ito, T. Bessho, M. Gratzel, Journal of the American Chemical Society 127 (2005) 16835.
[4] Y. Numata, S.P. Singh, A. Islam, M. Iwamura, A. Imai, K. Nozaki, L. Han, Advanced Functional Materials 23 (2013) 1817.
[5] T. Funaki, H. Funakoshi, O. Kitao, N. Onozawa-Komatsuzaki, K. Kasuga, K. Sayama, H. Sugihara, Angewandte Chemie-International Edition 51 (2012) 7528.
[6] S.H. Wadman, J.M. Kroon, K. Bakker, R.W.A. Havenith, G.P.M. van Klink, G. van Koten, Organometallics 29 (2010) 1569.
[7] A. Yella, H.-W. Lee, H.N. Tsao, C. Yi, A.K. Chandiran, M.K. Nazeeruddin, E.W.-G. Diau, C.-Y. Yeh, S.M. Zakeeruddin, M. Graetzel, Science 334 (2011) 629.
[8] A. Hagfeldt, G. Boschloo, L. Sun, L. Kloo, H. Pettersson, Chemical Reviews 110 (2010) 6595.
[9] P.G. Bomben, T.J. Gordon, E. Schott, C.P. Berlinguette, Angewandte Chemie-International Edition 50 (2011) 10682.
[10] T. Funaki, H. Funakoshi, O. Kitao, N. Onozawa-Komatsuzaki, K. Kasuga, K. Sayama, H. Sugihara, Angewandte Chemie International Edition 51 (2012) 7528.
[11] M.A. Baldo, S. Lamansky, P.E. Burrows, M.E. Thompson, S.R. Forrest, Applied Physics Letters 75 (1999) 4.
[12] S. Lamansky, P. Djurovich, D. Murphy, F. Abdel-Razzaq, H.E. Lee, C. Adachi, P.E. Burrows, S.R. Forrest, M.E. Thompson, Journal of the American Chemical Society 123 (2001) 4304.
[13] A. Tsuboyama, H. Iwawaki, M. Furugori, T. Mukaide, J. Kamatani, S. Igawa, T. Moriyama, S. Miura, T. Takiguchi, S. Okada, M. Hoshino, K. Ueno, Journal of the American Chemical Society 125 (2003) 12971.
[14] E. Holder, B.M.W. Langeveld, U.S. Schubert, Advanced Materials 17 (2005) 1109.
[15] E.I. Mayo, K. Kilsa, T. Tirrell, P.I. Djurovich, A. Tamayo, M.E. Thompson, N.S. Lewis, H.B. Gray, Photochemical and Photobiological Sciences 5 (2006) 871.
[16] Z. Ning, Q. Zhang, W. Wu, H. Tian, Journal of Organometallic Chemistry 694 (2009) 2705.
[17] Y.-J. Yuan, J.-Y. Zhang, Z.-T. Yu, J.-Y. Feng, W.-J. Luo, J.-H. Ye, Z.-G. Zou, Inorganic Chemistry 51 (2012) 4123.
[18] E. Baranoff, J.-H. Yum, M. Graetzel, M.K. Nazeeruddin, Journal of Organometallic Chemistry 694 (2009) 2661.
[19] K.R. Schwartz, R. Chitta, J.N. Bohnsack, D.J. Ceckanowicz, P. Miro, C.J. Cramer, K.R. Mann, Inorganic Chemistry 51 (2012) 5082.
[20] Q. Yan, Y. Fan, D. Zhao, Macromolecules 45 (2012) 133.
[21] A.J. Hallett, B.D. Ward, B.M. Kariuki, S.J.A. Pope, Journal of Organometallic Chemistry 695 (2010) 2401.
[22] B. Paulose, D.K. Rayabarapu, J.P. Duan, C.H. Cheng, Advanced Materials 16 (2004) 2003.
[23] D.K. Rayabarapu, B. Paulose, J.P. Duan, C.H. Cheng, Advanced Materials 17 (2005) 349.
[24] D.M. Kang, J.-W. Kang, J.W. Park, S.O. Jung, S.-H. Lee, H.-D. Park, Y.-H. Kim, S.C. Shin, J.-J. Kim, S.-K. Kwon, Advanced Materials 20 (2008) 2003.
[25] Dongdong Wang, Yong Wu, Bo Jiao, Hua Dong, Guijiang Zhou, Geng Wang, Zhaoxin Wu, Organic Electronics 14 (2013) 2233.
[26] Z.-S. Wang, H. Kawauchi, T. Kashima, H. Arakawa, Coordination Chemistry Reviews 248 (2004) 1381.
[27] J.-S. Ni, K.-C. Ho, K.-F. Lin, Journal of Materials Chemistry A 1 (2013) 3463.
[28] A. Anthonysamy, Y. Lee, B. Karunagaran, V. Ganapathy, S.W. Rhee, S. Karthikeyan, K.S. Kim, M.J. Ko, N.G. Park, M.J. Ju, J.K. Kim, Journal of Materials Chemistry 21 (2011) 12389.
[29] T.J.K. Findley, D. Sucunza, L.C. Miller, D.T. Davies, D.J. Procter, Chemistry – a European Journal 14 (2008) 6862.